Structural and Functional Characterization of the Clostridium perfringens N-Acetylmannosamine-6-phosphate 2-Epimerase Essential for the Sialic Acid Salvage Pathway

Marie-Cécile Pélissier, Corinne Sebban-Kreuzer, Françoise Guerlesquin, James A Brannigan, Yves Bourne, Florence Vincent

THE JOURNAL OF BIOLOGICAL CHEMISTRY VOL. 289, NO. 51, pp. 35215–35224, December 19, 2014

Structural and Functional Characterization of the *Clostridium perfringens N*-Acetylmannosamine-6-phosphate 2-Epimerase Essential for the Sialic Acid Salvage Pathway*

Received for publication, August 11, 2014, and in revised form, October 2, 2014 Published, JBC Papers in Press, October 15, 2014, DOI 10.1074/jbc.M114.604272

Marie-Cécile Pélissier[‡§1], Corinne Sebban-Kreuzer[¶], Françoise Guerlesquin[¶], James A. Brannigan[‖], Yves Bourne[‡§], and Florence Vincent[‡§2]

From the [‡]Aix-Marseille University, AFMB UMR7257, 163 avenue de Luminy 13288 Marseille, France, the [§]CNRS, AFMB UMR7257, 163 avenue de Luminy, 13288 Marseille, France, the [¶]Laboratoire d'Ingénierie des Systèmes Macromoléculaires, CNRS UMR7255, Aix-Marseille Université, 31 chemin Joseph Aiguier, 13402 Marseille Cedex 20, France, and the [‖]Department of Chemistry, Structural Biology Laboratory, University of York, Heslington, York YO10 5DD, United Kingdom

Background: The bacterial ManNAc-6P 2-epimerase (NanE) is essential for sialic acid salvage.
Results: Crystal structures of NanE in complex with substrate/product coupled to ^{1}H NMR kinetics on wild-type and variants elucidate the C2-epimerization mechanism.
Conclusion: A single lysine catalyst acts as a one-base mechanism for the C2-epimerization reaction interconverting ManNAc-6P to GlcNAc-6P.
Significance: A novel deprotonation/reprotonation mechanism involving a single flexible lysine is described.

Pathogenic bacteria are endowed with an arsenal of specialized enzymes to convert nutrient compounds from their cell hosts. The essential *N*-acetylmannosamine-6-phosphate 2-epimerase (NanE) belongs to a convergent glycolytic pathway for utilization of the three amino sugars, GlcNAc, ManNAc, and sialic acid. The crystal structure of ligand-free NanE from *Clostridium perfringens* reveals a modified triose-phosphate isomerase (β/α)$_8$ barrel in which a stable dimer is formed by exchanging the C-terminal helix. By retaining catalytic activity in the crystalline state, the structure of the enzyme bound to the GlcNAc-6P product identifies the topology of the active site pocket and points to invariant residues Lys^{66} as a putative single catalyst, supported by the structure of the catalytically inactive K66A mutant in complex with substrate ManNAc-6P. ^{1}H NMR-based time course assays of native NanE and mutated variants demonstrate the essential role of Lys^{66} for the epimerization reaction with participation of neighboring Arg^{43}, Asp^{126}, and Glu^{180} residues. These findings unveil a one-base catalytic mechanism of C2 deprotonation/reprotonation via an enolate intermediate and provide the structural basis for the development of new antimicrobial agents against this family of bacterial 2-epimerases.

Clostridium perfringens (*Clope*)[3] is a Gram-positive anaerobic bacterium commonly found in soils and sediments as well as in the gastrointestinal tract of most mammals. In some cases, *Clope* can become pathogenic and cause gastrointestinal diseases such as food poisoning and necrotic enteritis in humans (1). Besides these foodborne infections, *Clope* is the most common cause of gas gangrene, a life-threatening infection of muscle tissue in humans. *Clope* is a prolific producer of toxins and secreted virulence factors (2–4). In addition to the major toxins, *Clope* produces various minor toxins or enzymes and can release sialic acids from a variety of sialoglycoconjugates attached to eukaryotic cells. Once inside the cells, the sialylated compounds are further degraded into nutrients or biosynthetic precursors. Sialic acids are especially abundant in the intestinal tract, where they represent a major constituent of mucins and play a role in cell wall synthesis and pathogenesis (5–7). Utilization of sialic acid as a carbon source for growth has been demonstrated for the pathogenetic *Staphylococcus aureus* bacteria (8) as well as *Streptococcus pneumoniae* (9), and the importance of sialic acid catabolism in pathogenic bacteria has been documented for the foodborne enteropathogen *Vibrio vulnificus* (10).

In *Clope*, metabolism of imported sialic acid into fructose 6-phosphate is enabled by the gene products of the sialic acid-inducible nan operon that encodes a sialic acid lyase (NanA) and a *N*-acetylmannosamine-6-phosphate 2-epimerase (NanE) (11). Although the NanE 2-epimerase has been partially purified from *Aerobacter cloacae* (12), the 2-epimerase activity of the *Escherichia coli* enzyme was confirmed using radiolabeled ManNAc-6P (13). In the Gram-negative *Bacteroides* species, utilization of sialic acid requires an unrelated ManNAc/*N*-acetylglucosamine (NAG) 2-epimerase that possesses more similarity to the mammalian renin-binding protein than to other bacterial 2-epimerases of the NanE family (14). With the exception of NanE, proteins encoded by the nan operon display significant homology to mammalian proteins. Hence, NanE appears to be a very conserved protein among Gram-positive

* This work was supported in part by the CNRS and French Infrastructure for Integrated Structural Biology (FRISBI) Grant ANR-10-INSB-05-01.
[1] Present address: EMBL Hamburg, c/o DESY Notkestraße 85, 22603 Hamburg, Germany.
[2] To whom correspondence should be addressed: Laboratoire AFMB, CNRS, 163 avenue de Luminy, 13288 Marseille, France. Tel.: 0033-4-921825566; Fax: 0033-4-91266720; E-mail: florence.vincent@afmb.univ-mrs.fr.
[3] The abbreviations used are: Clope, *Clostridium perfringens*; NanE, *N*-acetylmannosamine-6-phosphate 2-epimerase; NanA, sialic acid lyase; NAG, *N*-acetylglucosamine; LIC, ligation independent cloning; Bistris propane, 1,3-bis[tris(hydroxymethyl)methylamino]propane.

and Gram-negative bacteria and can be considered as a potential target for development of broad-spectrum antimicrobial drugs.

Among the mechanistic strategies employed by carbohydrate epimerases, the deprotonation/reprotonation mechanism appears to be the most frequent for those acting on free sugars via a "one-base" *versus* "two-base" catalytic mechanism (15–18). Although the mechanistic aspects of several unrelated carbohydrate epimerases have been deciphered, the NanE-catalyzed epimerization reaction mechanism has not yet been elucidated. In a further step toward providing insights into the molecular mechanisms of this family of sugar 2-epimerases, we report the crystal structures of the ligand-free and product-bound forms of the NanE 2-epimerase from *Clope* (CpNanE) in the 1.45–1.9-Å resolution range. The structure of the K66A mutant in complex with the ManNAc-6P substrate reveals an unprocessed substrate bound to the active site pocket, supporting a dual catalytic role for the invariant residue Lys^{66} to perform a one-base catalytic mechanism of C2 deprotonation/reprotonation via an enolate intermediate. Complementary ^1H NMR kinetics experiments performed on wild-type and four active site mutants of CpNanE confirm the essential catalytic role of Lys^{66} for the epimerization reaction and reveal the participation of the surrounding residues Arg^{43}, Asp^{126}, and Glu^{180}.

MATERIALS AND METHODS

Cloning and Gene Expression—The entire coding sequence of NanE (UniProtKB/Swiss-Prot Q8XNZ3.1) was amplified by polymerase chain reaction (PCR) from *C. perfringens* strain 13 genomic DNA using Vent DNA polymerase (New England Biolabs) and complementary gene-specific primers to which were appended sequences to facilitate ligation independent cloning (LIC) (19). The PCR amplification product was treated with T4 DNA polymerase in the presence of dATP to generate 5′ single-stranded overhangs at both ends of the fragment, through the enzymes combined 3′-5′ exonuclease and DNA polymerase activities. Complementary 5′ single-stranded overhangs were generated in LIC-adapted pET-28a by cleavage with the restriction endonuclease BseRI and treatment with T4 DNA polymerase in the presence of dTTP. The kanamycin-resistant vector and PCR products were annealed and the resulting plasmid was transformed in *E. coli* NovaBlue cells (Novagen). The pET-YSBLIC vector confers an N-terminal MGSSHHHHHH FLAG extension (20). The DNA sequence of the gene insert was confirmed and the pET-YSBLIC*nanE* plasmid was transformed into *E. coli* Rosetta (Novagen) to confer additional tRNA genes and enhance protein expression.

Mutagenesis and Protein Production—Directed mutagenesis was performed on the plasmid coding NanE of *C. perfringens* (CpNanE) using the QuikChange Site-directed Mutagenesis Kit (Stratagene) to introduce the K66A, R43A, D126S, and E180A mutations in the coding sequence of the protein. The correct sequences of the four plasmids were confirmed by DNA sequencing. Plasmids were transformed into the *E. coli* strain Rosetta (DE3) pLysS. Bacteria were grown in LB medium supplemented with antibiotics at 37 °C until the A_{600} reached 0.6. Protein expression was induced by adding isopropyl β-D-thiogalactoside to a final concentration of 1 mM, and the culture was further incubated for 4 h at 30 °C. Cells were harvested by centrifugation, resuspended in lysis buffer (50 mM Tris-HCl, pH 8.0, 300 mM NaCl, 10 mM imidazole, 0.25 mg/ml of lysozyme, and 1 mM phenylmethylsulfonyl fluoride) and frozen at −80 °C. The bacterial suspension was thawed and incubated at 4 °C for 30 min after addition of 10 μg/ml of DNase and 20 mM $MgSO_4$ and completely disrupted by sonication. The lysate was clarified by centrifugation and the soluble fraction applied on a 5-ml Ni^{2+} chelating column (GE Healthcare). His-tagged proteins were eluted with 250 mM imidazole in 50 mM Tris-HCl, pH 8.0, and 300 mM NaCl. NanE-containing fractions were concentrated and purified by size exclusion chromatography on a Superdex 200 26/60 column (GE Healthcare) in their final buffer (10 mM Tris-HCl, pH 8.0, NaCl 200 mM). Because CpNanE lacks tryptophan residues, the protein concentration was estimated by the Bradford colorimetric method using bovine serum albumin as a standard (Bio-Rad).

The native CpNanE, and the four $CpNanE^{K66A}$, $CpNanE^{R43A}$, $CpNanE^{D126S}$, $CpNanE^{E180A}$ mutants were concentrated to 20–75 mg/ml by ultrafiltration, and stored at 4 °C. Purified proteins were analyzed by SDS-PAGE and further characterized by MALDI-TOF mass spectrometry, circular dichroism, and dynamic light scattering. Circular dichroism spectra of the four mutated variants were comparable with that of wild-type CpNanE, confirming their correct folding (data not shown).

Measurements of 2-Epimerase Activity by ^1H NMR Spectroscopy—Real time ^1H NMR spectra were recorded at 37 °C on a Bruker AvanceIII 600 spectrometer equipped with a TCI cryoprobe using water presaturation. Each sample contained 500 μl of ManNAc-6P in D_2O at various concentrations (4000, 3000, 2000, 1000, 800, 600, 300, 200, 150, and 100 μM) and β-alanine at a concentration approximately twice that of the substrate. At $t = 0$, 5 μl of enzyme (0.8 μM for CpNanE; 89 μM for $CpNanE^{K66A}$; 100 μM for $CpNanE^{R43A}$, $CpNanE^{E180A}$ and $CpNanE^{D126S}$ concentration) was added to the saccharide sample for a series of one-dimensional spectra during 40 min. Disappearance of ManNAc-6P was measured by integrating the peak area corresponding to the acetyl-CH_3 signal over the course of the reaction. For all experiments, a fixed concentration of β-alanine was used as an internal reference. The rate of disappearance of ManNAc-6P was calculated relative to the initial value of the substrate at a given concentration, using Microsoft Excel. Kinetic parameters (K_m and k_{cat}) were determined using non-regression fitting to the Michaelis-Menten equation (SigmaPlot-SYSTAT software).

Crystallization and Data Collection—Crystallization experiments were achieved using the vapor diffusion method at 20 °C. Crystals of native CpNanE were obtained in hanging drops by mixing equal volumes of a 20 mg/ml of protein solution and a well solution consisting of 0.1 M sodium cacodylate, pH 6.5, 0.2 M calcium acetate, 24.5% (w/v) PEG 2K MME, and 5% (v/v) PEG 400. Crystals of the apoenzyme were incubated for 2 min in the mother liquor supplemented with 30% PEG 2K MME, and then immediately flash-cooled and stored in liquid nitrogen. For the CpNanE·GlcNAc-6P complex, crystals of apo CpNanE were soaked for 2 min in the same cryoprotectant solution supplemented with solid ManNAc-6P before being flash-cooled.

TABLE 1
Data collection and refinement statistics

	NanE apo	NanE/GlcNAc-6P	NanE^{K66A}/ManNAc-6P
Crystal parameters			
Space group	*P*1	*P*1	$P2_1$
Cell dimensions			
Parameters *a*,*b*,*c* (Å) and α, β, γ (°)	36.7, 75.5, 82.2 90.2, 90, 92.8	36.7, 75.6, 82.2 89.9, 89.9, 92.9	36.7, 82.1, 75.2 90, 92.5, 90
No. of mol/AU	4	4	2
Data quality			
Wavelength (Å)	0.9792 (ID14EH3)	0.9792 (ID23EH1)	0.9792 (ID23EH1)
Resolution of data (Å) (outer shell)	82–1.7 1.8–1.7	50–1.9 2.0–1.9	42–1.45 1.5–1.45
Unique relfections	48,011	63,337	78,204
R_{merge}[a] (outer shell)	0.152 (0.339)	0.080 (0.418)	0.060 (0.461)
Mean $I/\sigma I$ (outer shell)	8.9 (2)	10 (1.5)	18 (4.3)
Completeness (outer shell) %	96.6 (77)	91 (85.9)	99.3 (95.8)
Multiplicity (outer shell)	4 (2.7)	1.9 (1.8)	7 (5.9)
Refinement			
Protein atoms	7113	7158	3629
Solvent waters	1115	999	498
Ligand + ions	12	80	40
R_{cryst}[b]	0.15	0.185	0.14
R_{free}[c]	0.185	0.248	0.169
Root mean square deviation 1–2 bonds (Å)	0.015	0.017	0.015
Root mean square deviation 1–3 angles (°)	1.5	1.6	1.6
PDB accession code	4UTT	4UTW	4UTU

[a] $R_{merge} = (\Sigma_{hkl} \Sigma_i |I_{hkl} - (I_{hkl})|/\Sigma_{hkl} \Sigma_i [I_{hkl}])$.
[b] $R_{cryst} = \Sigma_{hkl} ||F_o| - |F_c||/\Sigma_{hkl} |F_o|$.
[c] R_{free} is calculated for randomly selected reflections excluded from refinement.

Crystals of the CpNanE^{K66A} mutant appeared in sitting drops using the PACT premier crystallization kit (Molecular Dimensions Ltd.) with a 70 mg/ml of protein solution and 0.1 M propionic acid, cacodylate, Bistris propane buffer, pH 8.0, and 25% (w/v) PEG 1500 as a reservoir solution. For the CpNanE^{K66A}·ManNAc-6P complex, crystals were briefly soaked in a solution consisting of the reservoir solution supplemented with 50% (v/v) PEG 400 and tiny amounts of powdered ManNAc-6P. Diffraction data were all collected at the ESRF (European Synchrotron Radiation Facility, Grenoble, France). Data were processed and scaled using MOSFLM (21) and SCALA (22).

Model Building and Structure Refinement—The structure of ligand-free CpNanE was solved by molecular replacement, using MOLREP (23), with NanE from *Streptococcus pyogenes* (50.2% sequence identity with CpNanE) as a search model (Protein Data Bank accession code 1YXY). The rotation and translation functions yielded 4 unambiguous solutions corresponding to 4 molecules in the asymmetric unit. The electron density map calculated from the model was of sufficient quality to trace 95.5% of the molecule using the Arp-Warp program (24). The model was further refined using the REFMAC program from the CCP4 suite (25). All manual refitting was done with the program Coot (26). The electron density was of sufficient quality to allow us to build 8 additional residues comprising the His_6 tag and an extra residue pair (Ser-Gly) arising from the expression vector. The final model of apo CpNanE contains 7113 non-hydrogen protein atoms, 1115 water molecules, 8 chlorine ions, and 4 acetate molecules. The structure of apo CpNanE was used as a template to solve the structures of the CpNanE·GlcNAc-6P complex and CpNanE^{K66A}·ManNAc-6P complex using MOLREP (27). Refinement of these two ligand-bound structures was performed using the REFMAC program (25). Data collection and refinement statistics are summarized in Table 1. Stereochemistry of the three refined structures was assessed with the program PROCHECK (28). A comparative analysis of the three CpNanE structures and structural homologs was performed using the program Coot (29).

RESULTS

Overall Structure of CpNanE—The structure of ligand-free CpNanE was solved by molecular replacement using a monomer of the homologous NanE from *S. pyogenes* and refined to 1.7-Å resolution. CpNanE consists of a single domain that adopts a modified triose-phosphate isomerase $(\beta/\alpha)_8$ barrel-fold, in which the C-terminal α-helix projects away from the barrel instead of packing against the β-sheet (Fig. 1, *A* and *B*). In turn, a tightly associated dimer is formed, such that the two C-terminal helices are swapped, each of them packing against the β-sheet of the neighboring molecule (Fig. 1*C*). The dimeric assembly, with a buried surface of 1590 Å^2 per subunit to a 1.4-Å probe radius, was confirmed in solution by gel filtration, dynamic light scattering, and native PAGE analysis (data not shown).

In each subunit, the triose-phosphate isomerase barrel is capped by an additional short helix (α0) at its bottom and is surrounded by short loops, whereas the extended loop regions, out of the β2-α2 loop, shape a deep active site pocket at the C-terminal end (Fig. 1, *A*, *B*, and *D*). On one side of the barrel, the long β3-α3 loop, which harbors Lys^{66} and Tyr^{75} pointing toward the active site, could act as a lid that closes upon substrate binding, as observed for other β/α barrel enzymes (30, 31).

Structural Comparison—The overall structure and dimeric assembly of CpNanE are highly similar to those of the homologous enzymes from *S. pyo*genes (Protein Data Bank code 1YXY), *S aureus* (Protein Data Bank code 1Y0E), *and Salmonella enterica* (Protein Data Bank codes 3IGS and 3Q58), resulting in root mean square deviation values in the 1.3–1.1 Å range for 218 eq Cα atoms (calculated with SSM program (32)).

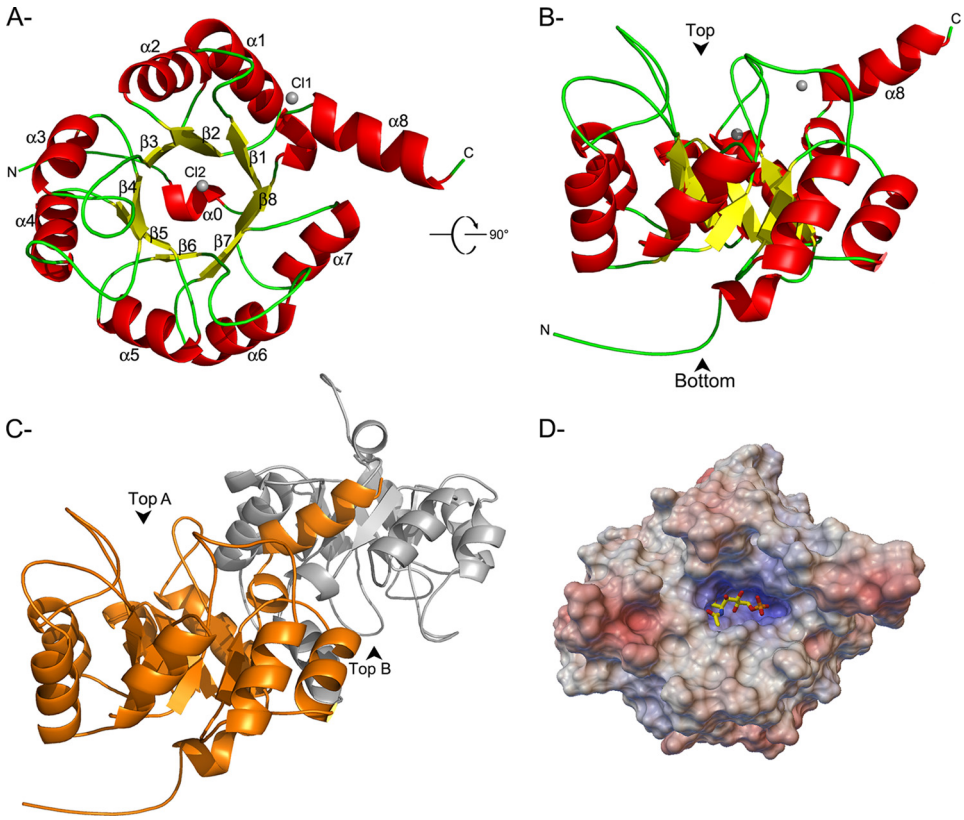

FIGURE 1. **Overall structure of NanE.** *A* and *B*, orthogonal views of the CpNanE structure, colored according to the type of secondary structures. The dominant α-β barrel structure hosts two chlorine ions, one (labeled Cl2) in the active site and the other (Cl1) at the periphery of the α/β barrel. *C*, domain-swapped dimeric assembly showing the interchange of the C-terminal helices. Secondary structure elements are numbered α0 to α8 and β1 to β8. *D*, electrostatic potential mapped on the molecular surface of a subunit of CpNanE^{wt} in complex with GlcNAc-6P is shown at −5 kT/e (*red*) to +5 kT/e (*blue*). The surface was calculated with APBS (53) and drawn using the Python Molecular Viewer program (54).

The most obvious differences (up to 5.5 Å) are confined to the positions of the β6-α6 loop region and helix α4 located at one edge of the barrel.

A similar comparative analysis of the two ligand-bound structures of CpNanE with that of the unliganded form (root mean square deviation values of 0.13 and 0.19 Å for 220 Cα atoms) reveals a rigid active site architecture with similar side chain orientation within the active site pocket, indicating that the presence of the substrate/product or mutated residue does not affect the overall tertiary structure of the enzyme.

Substrate Binding Site—In the dimer, the two catalytic sites are spatially located on opposite faces, ~30 Å apart, preventing a cooperative role in catalytic efficiency. In each subunit, the active site pocket shows a marked electropositive character consistent with binding of a substrate bearing a phosphate anion (Fig. 1*D*).

Crystals of CpNanE soaked with the ManNAc-6P substrate show unambiguous electron density for the open-chain form of the GlcNAc-6P product tightly bound at the bottom of the active site pocket in a pseudo-cyclic conformation, demonstrating that the crystalline enzyme is fully active (Fig. 2*A*). With the exception of the O-3 hydroxyl pointing toward the solvent, an extensive hydrogen bond network stabilizes the GlcNAc-6P product (Fig. 2*C*). The three O-1, O-4, and O-5 hydroxyl groups of the GlcNAc moiety are tightly bound to four polar side chains (Gln^{14}, Arg^{43}, Glu^{180}, and Arg^{208}) lining the pocket. On one face of the sugar, a central water molecule is tightly bound in an ideal tetrahedral conformation and contributes to the stabilization of the pseudo-cyclic conformation via the C1 aldehyde and C5 hydroxyl atoms. On the opposite face, a second water molecule coordinates the O-5 hydroxyl and N-2 nitrogen in a boat-like conformation. The carbonyl oxygen of the *N*-acetyl group is bound to the Tyr^{75} phenolic hydroxyl, whereas the methyl group is stacked against the Tyr^{151} phenolic ring, providing a structural rationale for the fine specificity of CpNanE toward *N*-acetylated amino sugars. At the bottom of the active site, the phosphate group is tightly anchored between the β7 and β8 strands with the oxygen atoms tethered by an extensive hydrogen bonding network involving the backbone amide nitrogens of residues Arg^{182}, Gly^{203}, and Gly^{204} and 5 solvent molecules, confirming the key role of the phosphate group for positioning the substrate in the optimal conformation for catalysis. Such tight binding of the phosphate group is consistent with the lack of CpNanE activity on ManNAc (data not shown). Overlay of the active site of the CpNanE bound to GlcNAc-6P with that of NanE from *S. enterica* reveals a similar architecture of the active site. However, the position of GlcNAc-6P in the active site of NanE from *S. enterica* is located 10 Å from that observed in CpNanE, precluding a detailed analysis.

A well ordered ManNAc-6P substrate is bound in the active site of the CpNanE^{K66A} mutant and adopts a similar position, with preservation of the hydrogen bond network, as seen for the GlcNAc-6P product in wild-type enzyme (Fig. 2*B*). Inspection

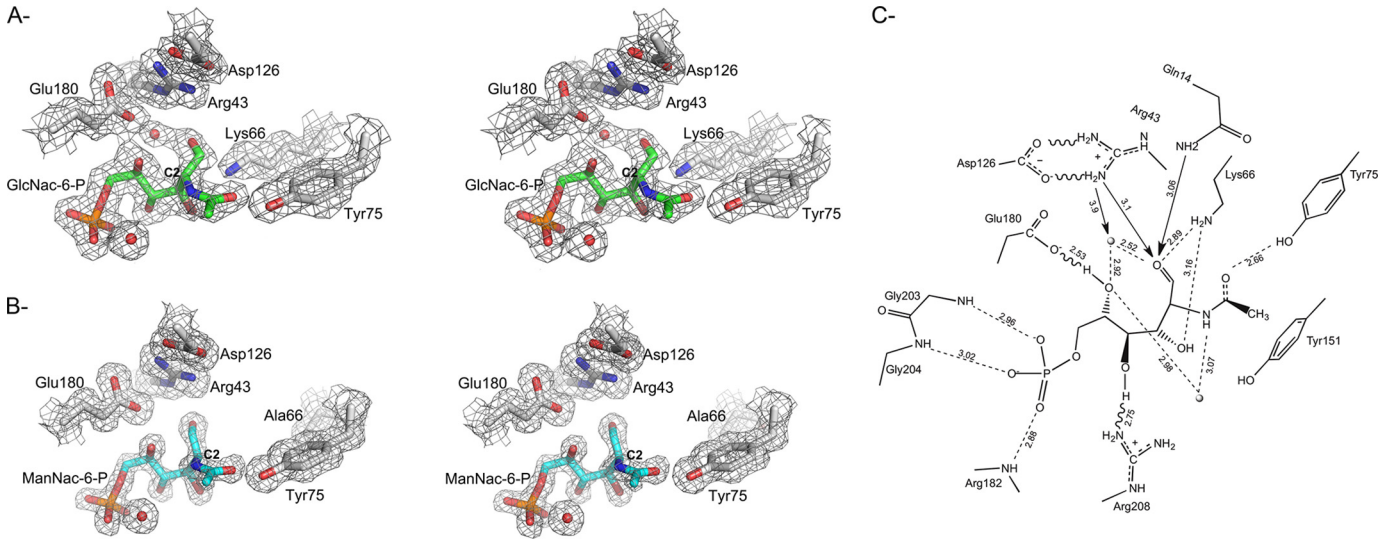

FIGURE 2. **Electron density maps in the active center.** *A*, stereoviews, shown in divergent ("walleyed") mode, of bound (*A*) GlcNAc-6P product in the active site of CpNanE^{wt}, showing catalysis in the crystal and (*B*) ManNAc-6P substrate in the active site of the CpNanE^{K66A} mutant. The maximum likelihood/σA weighted $2F_{obs} - F_{calc}$ electron densities are shown at 1.0 and 0.5 electrons/Å^2 for GlcNAc-6P and ManNAc-6P, respectively. Figures were drawn using PyMOL (55). *C*, schematic diagram of the active center of CpNanE with bound GlcNAc-6P and interacting side chains. Water molecules are shown as *small shaded spheres*. Hydrogen bonds and electrostatic interactions are shown by *dotted lines* and *wavy lines*, respectively, and some inter-atomic distances (Å) are indicated using *arrows* for clarity. Figure was drawn with CHEMDRAW (CambridgeSoft Corporation, Cambridge, MA).

of the active site of CpNanE reveals that the invariant Lys^{66} located within the long β3-α4 loop is the most likely candidate for the epimerization reaction (Figs. 2*C* and 3). Structural comparison of the substrate- and product-bound forms reveals that the ϵ-amino group of Lys^{66} is ideally positioned (2.5 Å) relative to the C2 atom of the ManNAc-6P substrate (Fig. 2, *A*–*C*). Due to the inversion of stereochemistry at the C2 stereogenic center, subtle differences are confined to the positions of the C1 aldehyde and C5 hydroxyl between the two stereoisomers, resulting in the lack of the central water molecule in the ManNAc-6P-bound form. In turn, the ManNAc-6P C1 aldehyde is bound to the Arg^{43} guanidinium group and the O-5 hydroxyl establishes hydrogen bonds with the Glu^{180} side chain and the second water molecule.

Real Time ^{1}H NMR Assays of CpNanE Activity—Because the NanE-catalyzed epimerization is strongly favored in the direction of fructose-6P (*GlcNAc-6P*) under normal growth conditions (13), we used ^{1}H NMR spectroscopy to follow conversion of ManNAc-6P into GlcNAc-6P as monitored by analyzing selected regions of the NMR spectra (Fig. 4, *A* and *B*). The characteristic NMR signal having two singlet peaks that correspond to the α- and β-anomers of the ManNAc-6P methyl group decreases during the time course of the CpNanE reaction. The resulting curve indicates non-linear progression of the reaction and permits determination of the initial rate of the reaction at different substrate concentrations. Analysis of these data are consistent with Michaelis-Menten kinetics (Fig. 4*C*). The apparent K_m value for ManNAc-6P is about 4.5 mM with a k_{cat} value of $\sim 1 \times 10^4$ min^{-1} (Table 2), in agreement with the low millimolar range reported for the human *N*-acetyl-D-glucosmine 2-epimerase, the *E. coli* galactose mutatotase from *E. coli* and the *Ruminococcus albus* cellobiose 2-epimerase (33–35).

We then used real time ^{1}H NMR to investigate the role of species-invariant ionizable side chains that interact with bound substrate and could be involved in the epimerization reaction (Fig. 3). Among the four point mutants (CpNanE^{K66A}, CpNanE^{R43A}, CpNanE^{E180A}, and CpNanE^{D126S}) that were assayed for enzyme activity, three (CpNanE^{R43A}, CpNanE^{D126S}, and CpNanE^{K66A}) displayed no detectable activity (even when using 100 times more enzyme than for wild-type CpNanE). Only the CpNanE^{E180A} mutant showed a residual activity due to a 60-fold lower catalytic efficiency (Table 2). These ^{1}H NMR kinetic data indicate that Arg^{43}, Asp^{126}, and Lys^{66} are crucial residues for the epimerization reaction and provide evidence for the participation of Glu^{180}. The key role of these four residues, and particularly Lys^{66} that could act as a one-base catalyst for C2 deprotonation/reprotonation epimerization mechanism, is consistent with the structural analysis of the substrate- and product-bound forms.

DISCUSSION

A Central Glycolytic Pathway—C. perfringens appears to be the first organism for which the intracellular sialic acid metabolism was reported (36). Since then, there has been an increased interest in the metabolism of sialic acid by bacterial pathogens, primarily due to the observed distribution pattern of genes required for sialic acid metabolism. These genes are confined to pathogenic and commensal bacteria having a close association with the human gut or lung in which the glycosylated mucin proteins from the mucus layer are extensively decorated with sialic acids (37). *C. perfringens* belongs to a limited group of pathogenic bacteria, along with *E. coli*, *Pasteurella multicoda*, *Haemophilus infuenzae*, *Bacteroides fragilis*, and *S. pneumoniae* for which sialic acid catabolism has been demonstrated (9, 14, 36, 38–40). These bacteria use the Nan operon composed of three enzymes: NanA (sialic acid lyase), NanE and NanK (*N*-acetylmannosamine kinase) to catabolize the sialic acid, and therefore use it as a source of carbon, nitrogen, or energy (37). The intestinal commensal bacterium *B. fragilis*,

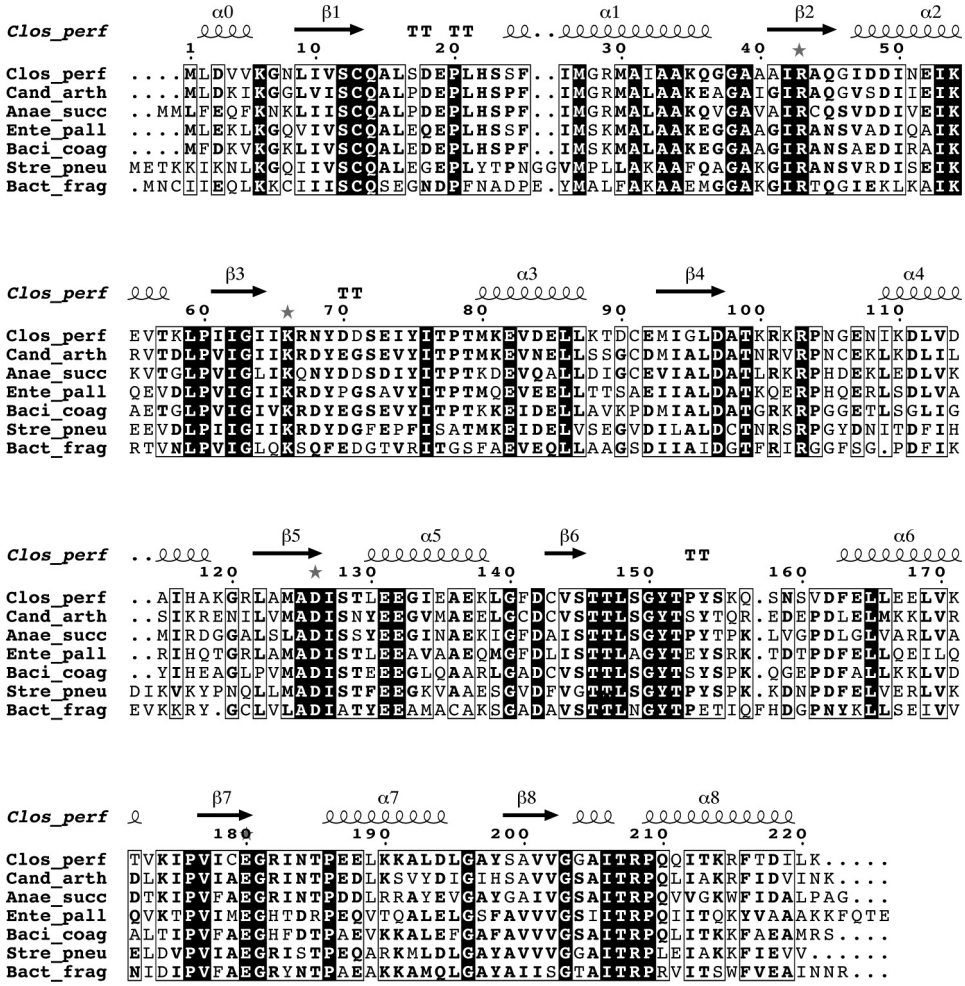

FIGURE 3. **Sequence alignment of representative NanE proteins.** The primary sequences of NanE proteins from *C. perfringens* (Clos_perf), *Candidatus arthromitus* (Cand_arth), *Enterococcus pallens* (Ente_pall), *B. fragilis* (Bact_frag), *S. pneumoniae* (Strep_pneu), *Bacillus coagulans* (Baci_coag), and *Anaerobiospirillum succiniciproducens* (Anae_succ) are aligned. The Clos_perf sequence corresponds to the gene product that has been used in this study. Secondary structure elements are labeled and shown *above* the alignment. The four invariant residues that have been mutated are shown with a *gray star*. The figure was generated using MultAlin and Esprit (56, 57).

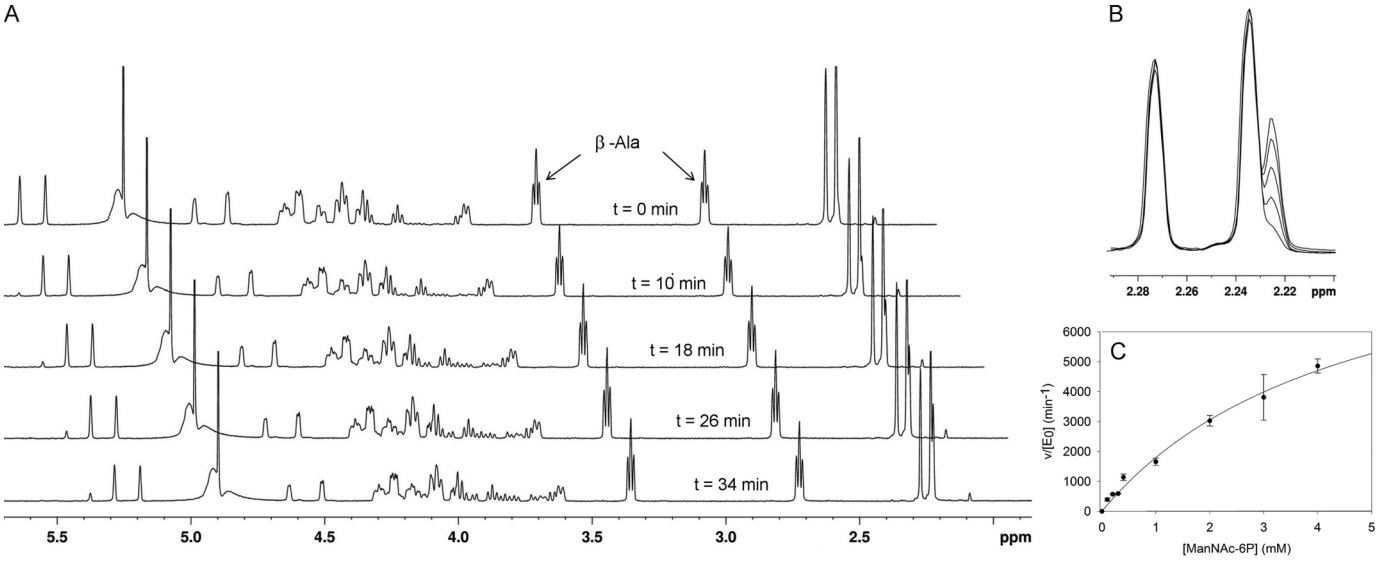

FIGURE 4. **Real time ^{1}H NMR analysis of CpNanE activity.** *A*, time course of ManNAc-6P (2 mM) epimerization by CpNanE in the presence of β-alanine (1 mM) as an internal standard was monitored. Selected regions of the spectra acquired between 0 and 34 min are shown. *B*, overlay of the spectral region from 2.2 to 2.3 ppm showing the disappearance of the characteristic peak for the ManNAc-6P methyl resonances *versus* appearance of GlcNAc-6P methyl resonance. *C*, initial velocities of ManNAc-6P epimerization by CpNanE in the presence of different concentrations of ManNAc-6P. A Michaelis-Menten curve was fitted using the formula: $v/[E]_0 = k_{cat}\,[S]/(K_m + [S])$.

TABLE 2
Kinetic parameters for wild type and CpNanE mutants for ManNAc-6P epimerization determined by ^{1}H NMR

Variants	Specific activity	k_{cat}	K_m	k_{cat}/K_m
	units/mg	min^{-1}	m_M	$min^{-1}\ m_M^{-1}$
$CpNanE^{wt}$	422 ± 61	10196 ± 1474	4.67 ± 1.05	2183
$CpNanE^{K66A}$	ND[a]			
$CpNanE^{R43A}$	ND			
$CpNanE^{D126S}$	ND			
$CpNanE^{E180A}$	7.9 ± 1.0	190 ± 25	5.19 ± 1.25	36.6

[a] ND, no detectable activity observed under assay conditions.

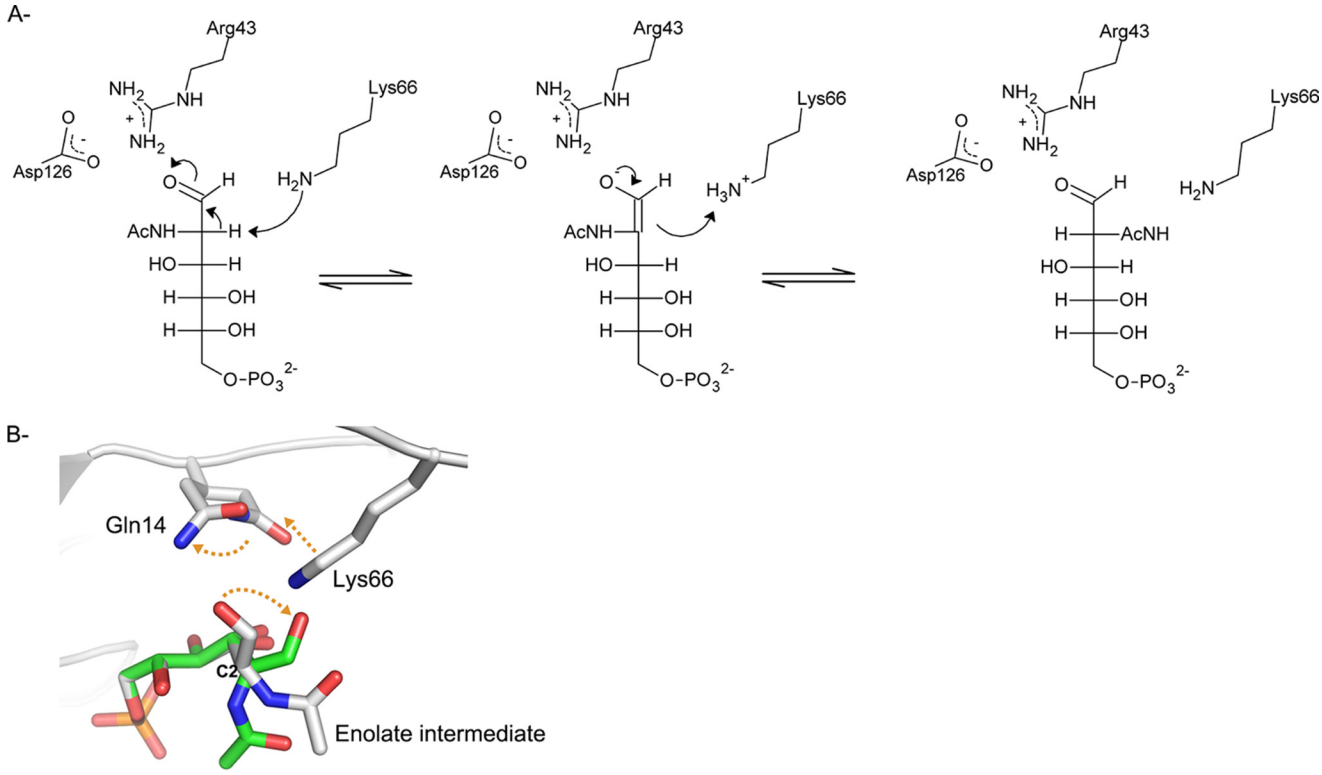

FIGURE 5. **Proposed catalytic mechanism of CpNanE.** *A*, once the C2 proton is abstracted by the base catalyst Lys^{66}, a negatively charged intermediate is stabilized by the salt bridge and Glu^{180}. Presence of the Asp^{126}-Arg^{43} salt bridge in proximity of the bound ManNAc-6P substrate reinforces the reactivity of Lys^{66}. A proton is donated by the same Lys^{66} catalyst to the enolate intermediate to yield the GlcNAc-6P product. *B*, a one-base mechanism for the interconversion of ManNAc-6P and GlcNAc-6P requires that Lys^{66} adjust its position in response to the rotation of the 1-keto intermediate around the C2-C3 bond. *Yellow dotted arrows* indicate the concerted motions. The figure was drawn with PyMOL (55).

however, does not encode NanK because the 2-epimerase (NanE) does not require a phosphorylated substrate to perform its metabolic reaction (14). The capacity of bacteria to catabolize sialic acid has a major influence on pathogenicity, resulting from a privileged access to a massive source of nutrients and a competitive asset over other sialic acid-independent pathogens or commensals (37, 41). Hence, the sialic acid catabolism has been shown to be essential for the colonization of the mouse colon by *E. coli* (42), *V. cholerae* (43), and *V. vulnificus* (44).

Implication of the Structures for the CpNanE Catalytic Mechanism—The present study investigates the molecular mechanism that allows NanE to specifically convert ManNAc-6P into GlcNAc-6P. This is a critical step in the catabolism of sialic acid as a carbon and energy source before the uptake by the GlcNAc-6P deacetylase (NagA) (45) and the GlcN-6P deaminase (NagB) enzymes (46) that convert GlcNAc-6P into fructose-6P for the first step in the glycolytic pathway (47). Inspection of the active site architecture of the $CpNanE^{wt}$ and $CpNanE^{K66A}$ structures suggests that a likely catalytic mechanism occurs via a deprotonation/reprotonation mechanism requiring formation of a planar enolate intermediate (Fig. 5*A*). In contrast to other epimerases that operate at "unactivated" stereocenters and are unable to employ such a direct mechanism due to the extreme pK_a value of the proton, this mechanistic strategy is preferred by enzymes acting at "activated" stereogenic centers adjacent to a carbonyl, carboxylic, or ester group, such as CpNanE. Yet, absence of a divalent metal ion in the active site of CpNanE rules out the elimination mechanism as seen in other cofactor-dependent bacterial epimerases (16). Besides, the proposed reaction mechanism implies formation of a cis-enediolate intermediate that carries a negative charge at the 2-oxygen, which has to be accommodated in an energetically favorable environment, ideally the so-called "oxyanion hole" from the β/α hydrolase-fold family made of backbone amides.

The pK_a value of the invariant Lys^{66}, as predicted by the PROPKA software (48), is slightly lower in the apoenzyme than

its reference value, and decreases drastically in the presence of substrate in the active site ($pK_a = 5.7$). At physiological pH, the deprotonated state of Lys^{66} should act as a Brønsted base for proton abstraction at the C2 position of the ManNAc-6P substrate. Moreover, Lys^{66} is well positioned (2.5 Å) below the substrate to convert it into a planar enolate anion intermediate after the first step of proton abstraction. Subsequently, the enol group has to be reduced from the opposite face to accomplish the inversion of the stereochemistry.

We choose to mutate three strictly invariant residues located in the active site among the sequences of the NanE family, namely Arg^{43}, Asp^{126}, and Glu^{180} (Fig. 3). Despite the total loss of activity caused by the substitution of residues Arg^{43} and Asp^{126} with Ala and Ser and the 60-fold decrease in the catalytic efficiency induced by the E180A mutation, none of these mutated residues is a likely candidate to act as an acid catalyst but could contribute to the lysine reactivity during the first step of catalysis. In $CpNanE^{WT}$ and $CpNanE^{K66A}$, a salt bridge occurs between the Asp^{126} and Arg^{43} side chains but is too distant (4.8 Å) from the substrate to be involved in the protonation reaction (Fig. 2*C*). We could predict that the R43A mutation would elevate the pK_a value of neighboring Lys^{66}, generating a less reactive lysine residue. The high calculated pK_a (~15) of Arg^{43} confirms its protonated state and the presence of a bound substrate does not alter its value. Substitution of Asp^{126} by a serine, however, results in a slight decrease of the pK_a of Arg^{43}, which indicates that Asp^{126} should be necessary for maintaining the protonated state of Arg^{43} (in addition to its stabilization). Because the Arg^{43} guanidinium group is within hydrogen-bonding distance of the O-1 aldehyde of the substrate, the anionic character of the C1 ketyl/oxyanion in the transient reactive intermediate would be stabilized by this interaction. This anionic character of the enolate intermediate is further supported by the presence of a chlorate ion (Cl2) bound at a similar position in the apo CpNanE structure (Fig. 1). Collectively, these data may explain the loss of activity of the two $CpNanE^{R43A}$ and $CpNanE^{D126S}$ variants. The Glu^{180} carboxyl group, which interacts with Arg^{43}, Asp^{126}, and the hydroxyl group on C5 of the substrate, is key to maintain an optimal conformation of the active site, supporting the residual activity of the $CpNan^{E180A}$ mutant.

The two $CpNanE^{K66A}$ and $CpNanE^{WT}$ structures reveal a common location of the open chain form of the sugar associated to a very rigid active site with very limited conformational adjustments of side chains lining the active site. Therefore we suggest that the plasticity required for the catalytic mechanism would solely lie on the enolate intermediate that should perform a 45 to 50° motion around the C2-C3 bond to allow the opposite face of the C2 (sp^2) atom to be reprotonated by Lys^{66} (Fig. 5, *A* and *B*). Modeling of the enolate intermediate in the active site shows that no particular residues would block this motion, taking into account that Lys^{66} should undergo a minimal displacement to let the aldehyde group of the enolate fill the "apical" space (Fig. 5*B*). In fact, small conformational flexibility of residues lining the active site is illustrated by the Gln^{14} side chain, which interacts with Lys^{66}. Gln^{14} adopts two alternate conformations in the active site of $CpNanE^{WT}$ but not in that of the $CpNanE^{K66A}$·ManNAc-6P complex (Fig. 5*B*). In one conformation of Gln^{14}, Lys^{66} can slightly move away to accommodate the rotated aldehyde group of the keto sugar. The fact that we could not evidence other conformational rotamers of Lys^{66} suggests that the enolate/C1-keto is a short-lived intermediate and that Lys^{66} restores its initial position very quickly. The role of a single lysine as a general base is quite unique to "cofactor-independent" sugar epimerases but has been observed in several other Mg^{2+}- or Ca^{2+}-dependent enzymes acting on carbohydrates (16, 49). Rotation of a C-C bond to form an enolate intermediate is well documented (50, 51), but not the driving force of this movement. In our case, alteration of the hydrogen bond network around the enolate intermediate could initiate rotation around the C2-C3 bond. Moreover, concerted motions of substrate and interacting residues have been suggested for the epimerization mechanism of the ADP-L-*glycero*-D-*manno*-heptose 6-epimerase from *E. coli*. In this proposed mechanism, the enzyme could employ a single flexible tyrosine residue for the deprotonation/reprotonation reaction and the substrate undergoes a 180° flip around the C5-C6 bond (52).

In summary, the structures of CpNanE and the catalytically inactive K66A mutant in complex with the product or substrate support a one-base mechanism for the epimerization reaction interconverting ManNAc-6P to GlcNAc-6P and identify Lys^{66} as a catalyst. Collectively, our findings identify the first deprotonation/reprotonation mechanism involving a single flexible lysine catalyst acting once as a Brønsted base on one stereoisomer and as an acid catalyst on the other. Availability of crystal structures of NanE complexes with inhibitors would complete the molecular determinants and mechanisms of this family of bacterial 2-epimerases with the aim to help structure-guided design of antimicrobial agents.

Acknowledgments—We thank Prof. Yuan Chuan Lee for providing us with a limited amount of ManNAc-6P. We also thank Olivier Bornet from the IMM NMR platform, CNRS-Marseille, for the setup up of kinetics experiments, Karine Alvarez for fruitful discussions about the kinetic experiments, and Aurélien Lebrun for help with the initial NMR experiments. We thank the ESRF staff for assistance with data collection.

REFERENCES

1. Brynestad, S., and Granum, P. E. (2002) *Clostridium perfringens* and foodborne infections. *Int. J. Food Microbiol.* **74,** 195–202
2. Hatheway, C. L. (1990) *Toxigenic clostridia*. *Clin. Microbiol. Rev.* **3,** 66–98
3. Rood, J. I. (1998) Virulence genes of *Clostridium perfringens*. *Annu. Rev. Microbiol.* **52,** 333–360
4. Petit, L., Gibert, M., and Popoff, M. R. (1999) *Clostridium perfringens*: toxinotype and genotype. *Trends Microbiol.* **7,** 104–110
5. Roggentin, P., Kleineidam, R. G., and Schauer, R. (1995) Diversity in the properties of two sialidase isoenzymes produced by *Clostridium perfringens* spp. *Biol. Chem. Hoppe Seyler* **376,** 569–575
6. Roggentin, P., Rothe, B., Kaper, J. B., Galen, J., Lawrisuk, L., Vimr, E. R., and Schauer, R. (1989) Conserved sequences in bacterial and viral sialidases. *Glycoconj. J.* **6,** 349–353
7. Shimizu, T., Ohtani, K., Hirakawa, H., Ohshima, K., Yamashita, A., Shiba, T., Ogasawara, N., Hattori, M., Kuhara, S., and Hayashi, H. (2002) Complete genome sequence of *Clostridium perfringens*, an anaerobic flesh-eater. *Proc. Natl. Acad. Sci. U.S.A.* **99,** 996–1001
8. Olson, M. E., King, J. M., Yahr, T. L., and Horswill, A. R. (2013) Sialic acid

catabolism in *Staphylococcus aureus*. *J. Bacteriol.* **195,** 1779–1788
9. Siegel, S. J., Roche, A. M., and Weiser, J. N. (2014) Influenza promotes pneumococcal growth during coinfection by providing host sialylated substrates as a nutrient source. *Cell Host. Microbe.* **16,** 55–67
10. Hwang, J., Kim, B. S., Jang, S. Y., Lim, J. G., You, D. J., Jung, H. S., Oh, T. K., Lee, J. O., Choi, S. H., and Kim, M. H. (2013) Structural insights into the regulation of sialic acid catabolism by the *Vibrio vulnificus* transcriptional repressor NanR. *Proc. Natl. Acad. Sci. U.S.A.* **110,** E2829–E2837
11. Walters, D. M., Stirewalt, V. L., and Melville, S. B. (1999) Cloning, sequence, and transcriptional regulation of the operon encoding a putative *N*-acetylmannosamine-6-phosphate epimerase (nanE) and sialic acid lyase (nanA) in *Clostridium perfringens*. *J. Bacteriol.* **181,** 4526–4532
12. Ghosh, S., and Roseman, S. (1965) The sialic acids: V. *N*-acyl-D-glucosamine 2-epimerase. *J. Biol. Chem.* **240,** 1531–1536
13. Ringenberg, M. A., Steenbergen, S. M., and Vimr, E. R. (2003) The first committed step in the biosynthesis of sialic acid by *Escherichia coli* K1 does not involve a phosphorylated *N*-acetylmannosamine intermediate. *Mol. Microbiol.* **50,** 961–975
14. Brigham, C., Caughlan, R., Gallegos, R., Dallas, M. B., Godoy, V. G., and Malamy, M. H. (2009) Sialic acid (*N*-acetyl neuraminic acid) utilization by *Bacteroides fragilis* requires a novel *N*-acetyl mannosamine epimerase. *J. Bacteriol.* **191,** 3629–3638
15. Allard, S. T., Giraud, M. F., and Naismith, J. H. (2001) Epimerases: structure, function and mechanism. *Cell Mol. Life Sci.* **58,** 1650–1665
16. Samuel, J., and Tanner, M. E. (2002) Mechanistic aspects of enzymatic carbohydrate epimerization. *Nat. Prod. Rep.* **19,** 261–277
17. Tanner, M. E. (2008) Transient oxidation as a mechanistic strategy in enzymatic catalysis. *Curr. Opin. Chem. Biol.* **12,** 532–538
18. Ito, S. (2009) Features and applications of microbial sugar epimerases. *Appl. Microbiol. Biotechnol.* **84,** 1053–1060
19. Aslanidis, C., and de Jong, P. J. (1990) Ligation-independent cloning of PCR products (LIC-PCR). *Nucleic Acids Res.* **18,** 6069–6074
20. Bonsor, D., Butz, S. F., Solomons, J., Grant, S., Fairlamb, I. J., Fogg, M. J., and Grogan, G. (2006) Ligation independent cloning (LIC) as a rapid route to families of recombinant biocatalysts from sequenced prokaryotic genomes. *Org. Biomol. Chem.* **4,** 1252–1260
21. Leslie, A. G. W., and Powell, H. R. (2007) Processing diffraction data with Mosflm. *Evolving Methods for Macromol. Crystallogr.* **245,** 41–51
22. CCP4, C. (1994) Collaborative Computational Project Number 4. *Acta Crystallogr. D Biol. Crystallogr.* **50,** 760–763
23. Vagin, A. A., and Teplyakov, A. (1997) MOLREP: an automated program for molecular replacement. *J. Appl. Crystallogr.* **30,** 1022–1025
24. Langer, G., Cohen, S. X., Lamzin, V. S., and Perrakis, A. (2008) Automated macromolecular model building for x-ray crystallography using ARP/wARP version 7. *Nat. Protoc.* **3,** 1171–1179
25. Murshudov, G. N., Vagin, A. A., and Dodson, E. J. (1997) Refinement of macromolecular structures by the maximum-likelihood method. *Acta Crystallogr. D Biol. Crystallogr.* **53,** 240–255
26. Emsley, P., Lohkamp, B., Scott, W. G., and Cowtan, K. (2010) Features and development of Coot. *Acta Crystallogr. D Biol. Crystallogr.* **66,** 486–501
27. Vagin, A. A., and Isupov, M. N. (2001) Spherically averaged phased translation function and its application to the search for molecules and fragments in electron-density maps. *Acta Crystallogr. D Biol. Crystallogr.* **57,** 1451–1456
28. Laskowski, R. A., MacArthur, M. W., Moss, D. S., and Thornton, J. M. (1993) PROCHECK: a program to check the stereochemical quality of protein structures. *J. Appl. Crystallogr.* **26,** 283–291
29. Emsley, P., and Cowtan, K. (2004) Coot: model-building tools for molecular graphics. *Acta Crystallogr. D Biol. Crystallogr.* **60,** 2126–2132
30. Joseph, D., Petsko, G. A., and Karplus, M. (1990) Anatomy of a conformational change: hinged "lid" motion of the triosephosphate isomerase loop. *Science* **249,** 1425–1428
31. Ochoa-Leyva, A., Barona-Gómez, F., Saab-Rincón, G., Verdel-Aranda, K., Sánchez, F., and Soberón, X. (2011) Exploring the structure-function loop adaptability of a $(\beta/\alpha)_8$-barrel enzyme through loop swapping and hinge variability. *J. Mol. Biol.* **411,** 143–157
32. Krissinel, E., and Henrick, K. (2004) Secondary-structure matching (SSM), a new tool for fast protein structure alignment in three dimensions. *Acta Crystallogr. D Biol. Crystallogr.* **60,** 2256–2268
33. Takahashi, S., Hori, K., Takahashi, K., Ogasawara, H., Tomatsu, M., and Saito, K. (2001) Effects of nucleotides on *N*-acetyl-D-glucosamine 2-epimerases (renin-binding proteins): comparative biochemical studies. *J. Biochem.* **130,** 815–821
34. Beebe, J. A., Arabshahi, A., Clifton, J. G., Ringe, D., Petsko, G. A., and Frey, P. A. (2003) Galactose mutarotase: pH dependence of enzymatic mutarotation. *Biochemistry* **42,** 4414–4420
35. Ito, S., Hamada, S., Ito, H., Matsui, H., Ozawa, T., Taguchi, H., and Ito, S. (2009) Site-directed mutagenesis of possible catalytic residues of cellobiose 2-epimerase from *Ruminococcus albus*. *Biotechnol. Lett.* **31,** 1065–1071
36. Nees, S., Schauer, R., and Mayer, F. (1976) Purification and characterization of *N*-acetylneuraminate lyase from *Clostridium perfringens*. *Hoppe-Seyler's Z. Physiol. Chem.* **357,** 839–853
37. Almagro-Moreno, S., and Boyd, E. F. (2009) Insights into the evolution of sialic acid catabolism among bacteria. *BMC Evol. Biol.* **9,** 118
38. Steenbergen, S. M., Lichtensteiger, C. A., Caughlan, R., Garfinkle, J., Fuller, T. E., and Vimr, E. R. (2005) Sialic acid metabolism and systemic pasteurellosis. *Infect. Immun.* **73,** 1284–1294
39. Vimr, E. R., and Troy, F. A. (1985) Identification of an inducible catabolic system for sialic acids (nan) in *Escherichia coli*. *J. Bacteriol.* **164,** 845–853
40. Severi, E., Randle, G., Kivlin, P., Whitfield, K., Young, R., Moxon, R., Kelly, D., Hood, D., and Thomas, G. H. (2005) Sialic acid transport in *Haemophilus influenzae* is essential for lipopolysaccharide sialylation and serum resistance and is dependent on a novel tripartite ATP-independent periplasmic transporter. *Mol. Microbiol.* **58,** 1173–1185
41. Smith, H. (2000) Questions about the behaviour of bacterial pathogens *in vivo*. *Philos. Trans. R. Soc. Lond. B Biol. Sci.* **355,** 551–564
42. Chang, D. E., Smalley, D. J., Tucker, D. L., Leatham, M. P., Norris, W. E., Stevenson, S. J., Anderson, A. B., Grissom, J. E., Laux, D. C., Cohen, P. S., and Conway, T. (2004) Carbon nutrition of *Escherichia coli* in the mouse intestine. *Proc. Natl. Acad. Sci. U.S.A.* **101,** 7427–7432
43. Almagro-Moreno, S., and Boyd, E. F. (2009) Sialic acid catabolism confers a competitive advantage to pathogenic vibrio cholerae in the mouse intestine. *Infect. Immun.* **77,** 3807–3816
44. Jeong, H. G., Oh, M. H., Kim, B. S., Lee, M. Y., Han, H. J., and Choi, S. H. (2009) The capability of catabolic utilization of *N*-acetylneuraminic acid, a sialic acid, is essential for *Vibrio vulnificus* pathogenesis. *Infect. Immun.* **77,** 3209–3217
45. Vincent, F., Yates, D., Garman, E., Davies, G. J., and Brannigan, J. A. (2004) The three-dimensional structure of the *N*-acetylglucosamine-6-phosphate deacetylase, NagA, from *Bacillus subtilis*: a member of the urease superfamily. *J. Biol. Chem.* **279,** 2809–2816
46. Vincent, F., Davies, G. J., and Brannigan, J. A. (2005) Structure and kinetics of a monomeric glucosamine 6-phosphate deaminase: missing link of the NagB superfamily? *J. Biol. Chem.* **280,** 19649–19655
47. Plumbridge, J., and Vimr, E. (1999) Convergent pathways for utilization of the amino sugars *N*-acetylglucosamine, *N*-acetylmannosamine, and *N*-acetylneuraminic acid by *Escherichia coli*. *J. Bacteriol.* **181,** 47–54
48. Rostkowski, M., Olsson, M. H., Søndergaard, C. R., and Jensen, J. H. (2011) Graphical analysis of pH-dependent properties of proteins predicted using PROPKA. *BMC Struct. Biol.* **11,** 6
49. Garron, M. L., and Cygler, M. (2010) Structural and mechanistic classification of uronic acid-containing polysaccharide lyases. *Glycobiology* **20,** 1547–1573
50. Fujiwara, T., Saburi, W., Matsui, H., Mori, H., and Yao, M. (2014) Structural insights into the epimerization of β-1,4-linked oligosaccharides catalyzed by cellobiose 2-epimerase, the sole enzyme epimerizing non-anomeric hydroxyl groups of unmodified sugars. *J. Biol. Chem.* **289,** 3405–3415
51. Seeholzer, S. H. (1993) Phosphoglucose isomerase: a ketol isomerase with aldol C2-epimerase activity. *Proc. Natl. Acad. Sci. U.S.A.* **90,** 1237–1241
52. Kowatz, T., Morrison, J. P., Tanner, M. E., and Naismith, J. H. (2010) The crystal structure of the Y140F mutant of ADP-L-glycero-D-manno-heptose 6-epimerase bound to ADP-beta-D-mannose suggests a one base mechanism. *Protein Sci.* **19,** 1337–1343

53. Baker, N. A., Sept, D., Joseph, S., Holst, M. J., and McCammon, J. A. (2001) Electrostatics of nanosystems: application to microtubules and the ribosome. *Proc. Natl. Acad. Sci. U.S.A.* **98,** 10037–10041
54. Sanner, M. F. (1999) Python: a programming language for software integration and development. *J. Mol. Graph. Model* **17,** 57–61
55. DeLano, W. L. (2002) *The PyMOL Molecular Graphics System*. DeLano Scientific, San Carlos, CA
56. Corpet, F. (1988) Multiple sequence alignment with hierarchical clustering. *Nucleic Acids Res.* **16,** 10881–10890
57. Gouet, P., Robert, X., and Courcelle, E. (2003) ESPript/ENDscript: extracting and rendering sequence and 3D information from atomic structures of proteins. *Nucleic Acids Res.* **31,** 3320–3323

Protein Structure and Folding:

Structural and Functional Characterization of the *Clostridium perfringens N*-Acetylmannosamine-6-phosphate 2-Epimerase Essential for the Sialic Acid Salvage Pathway

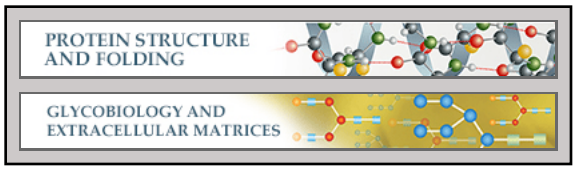

Marie-Cécile Pélissier, Corinne Sebban-Kreuzer, Françoise Guerlesquin, James A. Brannigan, Yves Bourne and Florence Vincent

J. Biol. Chem. 2014, 289:35215-35224.
doi: 10.1074/jbc.M114.604272 originally published online October 15, 2014